The pH dependence of the electrocatalytic nitrate reduction by tin-modified palladium(100) electrodes: Effects of structures of tin species and protonation of nitrite

Yang Deng [a, †], Masaru Kato [b, c *], Jinhang Zheng [c], Chuanping Feng [a], Ichizo Yagi [b, c *]

[a] *Key Laboratory of Groundwater Circulation and Environmental Evolution (China University of Geosciences (Beijing)), Ministry of Education, Beijing, 100083, China*

[b] *Faculty of Environmental Earth Science, Hokkaido University, N10W5, Kita-ku, Sapporo, 060-0810, Japan*

[c] *Graduate School of Environmental Science, Hokkaido University, N10W5, Kita-ku, Sapporo, 060-0810, Japan*

* Corresponding Authors:

masaru.kato@ees.hokudai.ac.jp (M. K.) and iyagi@ees.hokudai.ac.jp (I. Y.)

[†] Present address: *Department of Environmental Engineering, Peking University, The Key Laboratory of Water and Sediment Sciences, Ministry of Education, Beijing 100871, China*

Graphical Abstract

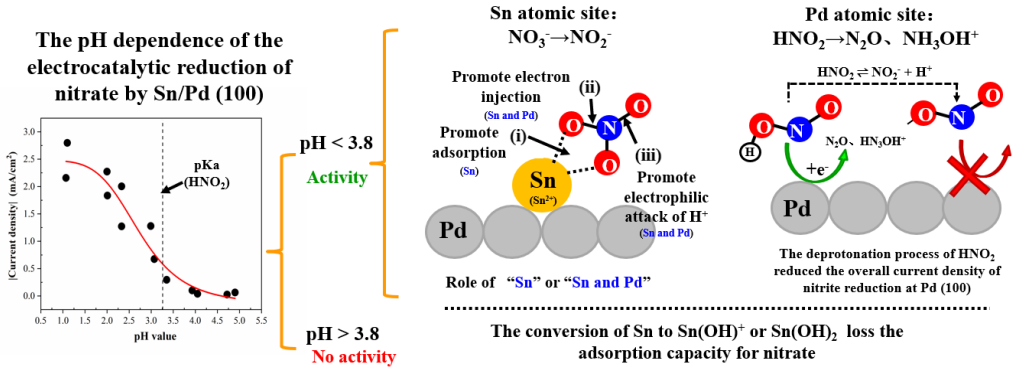

Highlights

- The Sn/Pd(100) electrode exhibits NO_3RR activity when the pH is below 3.8
- The form of Sn^{2+} (pH < 3.8) promotes NO_3^- adsorption on Sn site
- Combination of Sn and Pd reduces the LUMO energy of adsorbed nitrate molecule
- Protonation of NO_2^- is crucial to support its reduction on the surface of Pd(100)

Abstract

Nitrate is a common pollutant in groundwater and endangers drinking water safety. The electrocatalytic nitrate reduction using tin-modified palladium electrode (Sn/Pd) provided a promising alternative for nitrate removal. However, the pH effect on the nitrate reduction activity of Sn/Pd and its mechanistic insights are still unclear. In this study, Sn/Pd(100) single crystalline electrodes were used as a model electrode to understand the pH effect on its nitrate and nitrite reduction activity and mechanism. Sn/Pd(100) electrodes showed the nitrate reduction activity at pH < 3.8. DFT calculations suggest that Sn^{2+} site can be found on Pd(100) at pH < 3.8 and promote nitrate adsorption. The copresence of Sn and Pd sites can reduce the LUMO energy of the adsorbed nitrate molecule and decrease the van der Waals electrostatic potential of the O-N bond, which promotes electron injection and protonation to nitrate. At pH > 3.8, on the other hand, the formation of $Sn(OH)^+$ or $Sn(OH)_2$ can inhibit the adsorption of NO_3^- on Sn atoms, resulting in the disappearance of the electrocatalytic activity. Sn atomic sites mainly promote the reduction step of $NO_3^- \rightarrow NO_2^-$, and the subsequent NO_2^- reduction reaction occurs on Pd sites. The protonation of NO_2^- was crucial to the nitrite reduction on Pd(100) surface. The findings in this study would be useful to develop highly active electrocatalysts based on Sn and Pd materials for the nitrate reduction.

***Keywords*:**

Tin-modified palladium(100); Electrocatalysis; Nitrate reduction; Effect of tin structures; Effect of nitrite protonation

1. Introduction

As a common pollutant in groundwater, nitrate (NO_3) widely comes from fertilizer in agricultural activities [1], industrial wastewater leakage [2], landfill leachate infiltration [3]. Excessive nitrate in drinking water causes serious human diseases including blue baby disease, liver injury, and tumors [4]. Considering the hazard of nitrate, the maximum pollution level of nitrate is limited to 10 mg-N/L by US Environmental Protection Agency (USEPA) [5].

In recent years, electrochemical technology has been considered a feasible alternative for the nitrate removal due to its simple, stable, and efficient operation [6]. The efficiency of the electrochemical removal of nitrate depends on the electrocatalytic activity of the cathode for the nitrate reduction reaction (NO_3RR). The NO_3RR involves a continuous process of multi-electron transfer (Eq.1) [7] and produce a variety of reduction products including nitrite (NO_2^-), nitrous oxide (N_2O), nitrogen gas (N_2), and ammonia (NH_3):

$$NO_3^- \rightarrow NO_2^- \rightarrow NO \rightarrow N_2O \rightarrow N_2 \rightarrow NH_3 \quad (1)$$

The electrochemical NO_3RR is an interfacial process, and electrode materials such as single metal [8-10], alloy [11-13], and silicon-based materials [14-15] have been studied to control the reaction pathway of the NO_3RR. Among the reported materials, electrodes containing Pd are known to show high product selectivity for the NO_3RR to N_2 [16]. However, the Pd electrode itself shows almost no NO_3RR activity [17] and should be modified by other elements such as tin (Sn) as a promoter to reduce the

71 interfacial reaction barrier for the NO_3RR. Sn-modified Pd or alloy electrodes such as
72 Sn/Pd [17-19] and Sn/Pd-Pt [18-19] have been studied for the NO_3RR. A Sn/Pd/Au
73 electrode shows high catalytic NO_3RR activity in 0.1 M $HClO_4$, and its activity
74 depends on the joint action of Pd atom and Sn atom [20-21]. Sn/Pd electrodes are also
75 known that the NO_3RR is competitive with the adsorption of SO_4^{2-} in 0.1 M H_2SO_4
76 but does not affect the product composition [17]. Furthermore, Sn-modified Pd(111)
77 and Pd(100) single crystalline surfaces show the NO_3RR activity in acidic medium
78 (0.1 M $HClO_4$), and Sn/Pd(100) shows higher activity than Sn/Pd(111) [18-19]. The
79 NO_3RR activity of Sn-modified Pd electrodes has been mainly studied in acidic media
80 and it seems that pH values affect the NO_3RR activity of Sn/Pd electrodes. In the case
81 of Pt electrodes, pH can affect the protonation forms of nitrite and control the reaction
82 pathway for the nitrite reduction reaction (NO_2RR) [21]. However, pH effects on the
83 NO_3RR and NO_2RR activity of remain unclear for Sn/Pd(100) and Pd(100)
84 electrodes.

85 Herein, the pH dependence of NO_3RR activity of Sn/Pd(100) single crystalline
86 electrodes were analyzed by a combination of electrochemical measurement and
87 density functional theory (DFT) calculation. The effects of structures of tin species
88 and protonation of intermediate product nitrite for NO_3RR were discussed. The
89 findings of this study provided a reference for further understanding the nitrate
90 reduction process of Sn/Pd electrode, as well as the preparation and optimization of
91 electrode based on Sn/Pd for the NO_3RR.

2. Materials and methods

2.1. Samples and materials

The tin(II) chloride dihydrate (purity: 97.0%), sodium nitrate (purity: 99.0%), and sodium nitrite (purity: 98.5%) used in this study were purchased from Kanto Chemical Industries, Ltd. The perchloric acid (70%, purity: 99.999%) and sulfuric acid (purity: 99.999%) were purchased from Sigma-Aldrich. Pd wire (purity: 99.99%, 0.8 mmϕ) was used for the preparation of single crystalline electrodes. Milli-Q ultrapure water from a filtration system (MILLIPORE, USA) was used to prepare the electrolyte solution.

2.2. Electrode preparation

2.2.1 Preparation of Pd (100) single crystalline electrode

The preparation method of single crystalline electrodes was the same as that of our previous research [18]. A melted Pd bead at the end of Pd wire was obtained in methane-oxygen flame. After slow cooling, the single crystal bead was obtained and the (111) and (100) facets can be observed on the Pd bead. A (100) facet was aligned to be parallel to the baseplate by He-Ne laser reflection. After the (100) facet was aligned, the Pd bead was cut by a MC-201N cutting machine (MARUTO) and then polished by a ML-150P polishing machine (MARUTO) to be the mirror plane. After polishing, the single crystalline electrode was annealed at 1100–1200℃ for 4 h. Cyclic voltammograms (CVs) of the prepared electrodes were recorded in a 0.5 M H_2SO_4 aqueous solution and then compared with the reported CVs [22] to confirm the

113 successful preparation of Pd(100) electrodes.

114 **2.2.2 Preparation of Sn/Pd(100) electrode**

115 The surface of the Pd(100) electrode was modified with Sn by immersion process.
116 The Sn-containing solution used in this study was 0.1 mM $SnCl_2$ aqueous solution.
117 After the annealing in inductive heating furnace (EASY-HEAT model 0224, Ambrell)
118 under Ar atmosphere, cooling and quenching in milli-Q water, the Pd(100) electrode
119 covered with a droplet of Milli-Q water was transferred to the electrochemical cell,
120 and then, the electrochemical characterization of Pd(100) surface was carried out by
121 CV measurement in deaerated 0.5 M H_2SO_4 solution. When the chraracteristic CV of
122 clean Pd(100) electrode was obtained, the Pd(100) electrode with a droplet of 0.5 M
123 H_2SO_4 solution was immersed in 0.1 mM $SnCl_2$ solution for 1-30 s, then immediately
124 removed and rinsed by deaerated Milli-Q water, following by transferred to the
125 three-electrode electrochemical cell to measure the CV curves in the region of
126 underpotentially deposited hydrogen (H_{UPD}) desorption (< +0.5 V vs. RHE) [18]. The
127 Sn-coverage (θ_{Sn}) was calculated by hydrogen desorption Faradaic charge (mC)
128 before (Q_H^0) and after (Q_H) Sn-modification according to Eq. 2 [20].

129 $$\theta_{Sn} = \frac{Q_H^0 - Q_H}{Q_H^0} \times 100 \quad (2)$$

130 **2.3. Electrochemical analysis**

131 The CVs and linear sweep voltammograms (LSVs) were acquired by a HZ-7000
132 electrochemical measurement system (Hokuto Denko) controlled by a computer. In
133 this study, a three-electrode cell was constructed with Pt foil coated with platinum

black and Ag|AgCl (sat. KCl aq.) electrodes as the counter and reference electrodes, respectively. The Sn/Pd (100) electrode with different Sn-coverage was used as the working electrode. The potentials expressed in this study were converted into reversible hydrogen electrode (RHE) by Eq. 3.

$$E_{(RHE)} = E_{(Ag/AgCl)} + 0.197 + 0.0591 \times pH \quad (3)$$

The experimental conditions for exploring the nitrate reduction behavior of Sn/Pd(100) electrode and the nitrite reduction behavior of Pd(100) electrode under different pH were shown in Table S1 and Table S2. Each pH value was measured by a pH/ORP METER D-72 Tester (HORIBA, Japan).

2.4. Theoretical calculation

2.4.1 Calculation of Gibbs free energy

The initial structure model of Pd crystal had been given by Wyckoff [23], and published on the website of American Mineralogist Crystal Structure Database (http://rruff.geo.arizona.edu/AMS/amcsd.php) for open access. The molecular structure was constructed and optimized using BURAI 1.3 software (http://nisihara.wixsite.com/burai) and Quantum-ESPRESSO software ([24], https://www.quantum-espresso.org/). The Pd surface was simulated with 2×2 (100) cells. The ultrasoft Vanderbilt pseudopotential method with Perdew–Burke–Ernzerhof exchange-correlation functional was selected [25-26]. Using 500 eV as the plane-wave cutoff energy [27]. The vacuum thickness was set to 15 Å in calculations. The gaussian scheme was used for sampling the Brillouin zone and k-point grid of 2×2×1 [28]. The relaxations of the atoms were performed until the maximum force on

any atom was below 0.03 eV/Å. The minimum energy (E^{DFT}) (eV) of the structure can be obtained after optimization.

After the molecular structure optimization, the atomic coordinates of the lowest energy structure can be obtained. And then the .cube file containing the atomic coordinates of this structure can be obtained through the pp.x program (https://www.quantum-espresso.org/Doc/INPUT_PP.html) of Quantum-ESPRESSO software. After obtaining the .cube file, the input file of ORCA 5.0.0 software (https://orcaforum.kofo.mpg.de/) [29] can be generated by Multiwfn software (http://sobereva.com/multiwfn/) [30], and the zero point energy (*ZPE*) (eV) and entropy (*TS*) (eV) at 298.15 K can be obtained by Frequency calculation using ORCA 5.0.0 software with the b97-3c basis group.

The Gibbs free energy (*G*) (eV) was calculated by Eq. 4.

$$G = E^{DFT} + ZPE - TS \quad (4)$$

In this study, the correction of the adsorption Gibbs free energy change of NO_3^- in aqueous ($\Delta G(NO_3^-)$) was based on the method in reference [31]. Firstly, the Gibbs free energy change of gaseous HNO_3 ($\Delta G(HNO_3)$) was calculated. Then, the $\Delta G(NO_3^-)$ was corrected by considering two thermodynamic processes: (i) the conversion of HNO_3 (g) into liquid HNO_3 (HNO_3 (l)), and (ii) the dissociation of HNO_3 (l) into NO_3^-. Specifically, the Gibbs free energy change of HNO_3 (l) evaporation can be calculated from the Gibbs free energy difference (0.075 eV) between the standard products of HNO_3 in liquid phase and gas phase [32]. Moreover, the Gibbs free energy of HNO_3 (l) formed by NO_3^- in aqueous solution is 0.317 eV

[33]. Therefore, the correction process can be described as Eq. 5 (The unit in the equation is eV). In addition, the Gibbs free energy of electrons ($\Delta G(e^-)$) in the structures (Sn^{2+}/Pd(100) and $Sn(OH)^+$/Pd(100)) were corrected by using the result ($\Delta G(e^-)$ = -0.038 eV, 298.15 K, 1 bar [33]).

$$\Delta G(NO_3^-) = \Delta G(HNO_3) + 0.075 + 0.317 \quad (5)$$

2.4.2 Calculation of density of states (DOS)

The changes of DOS were calculated by the BURAI 1.3 software. The energy of the lowest unoccupied molecular orbital (LUMO) was determined at the position higher than the 0 eV vs E_f in the DOS diagram.

2.4.3 Calculation of van der Waals electrostatic potential (ESP)

In this study, ESP and extreme point were calculated by Multiwfn software [30]. Before using Multiwfn software for calculation, it is necessary to obtain the input file containing the basis function (such as the .molden file output from ORCA 5.0.0 software). Therefore, firstly the .molden file was obtained after optimizing the structure by ORCA 5.0.0 software. In addition, modify the [atoms] section in the molden file to the actual number of nuclear charges base on the Multiwfn standard manual before calculating ESP (http://sobereva.com/multiwfn/Multiwfn_manual.html).

2.5. Curve fitting analysis

The reduction current change of nitrate or nitrite at different pH is a dose-dependent reaction, and those kinds of reactions can be fitted by Logistic model [34]. In this

study, the Logistic model was fitted by the Origin software (OriginLab, USA), and the equation can be described as Eq. 6 (https://www.originlab.com/doc/Origin-Help/Logistic-FitFunc).

$$y = \frac{A_1 - A_2}{1 + \left(\frac{x}{x_0}\right)^p} + A_2 \quad (6)$$

Where, y represents the objective function value (in this study it was the reduction current density (mA/cm^2)), x is the independent variable (in this study it was the pH value). A_1 and A_2 is the maximum and minimum value (mA/cm^2) of y. x_0 represents the value of x when y equals half of A_2, and $-p$ is the slope of the curve at x = x_0.

In this study, we need to observe the pH value at the fastest decreasing of reduction current density that can be achieved by calculating the inflection point (x_1) of the curve (that is, the second derivative of y equals 0). According to the method of Origin software (https://www.originlab.com/doc/Origin-Help/Logistic-FitFunc), the relationship of x_1, x_0 and p can be described by Eq. 7. The curve fitting results and inflection point information were presented in Supporting Materials Table S5.

$$\left(\frac{x_1}{x_0}\right)^p = \frac{p-1}{p+1} \quad (7)$$

3. Results and discussion

3.1. Nitrate reduction behavior of Sn/Pd(100) at different pH values

In order to confirm the preparation of electrodes, CVs of Pt(100) and Sn/Pd(100) were recorded in 0.5 M H_2SO_4 aqueous solution under Ar (Fig. 1a). For the Pd(100) electrode, the current peaks corresponding to the adsorption and desorption of H_{UPD}

were observed at 0.25 V and 0.34 V vs. RHE, respectively, in a 0.5 M H_2SO_4 aqueous solution, which was consistent with the results previously reported [22]. For Sn/Pd(100), the surface modification with Sn decreased the current density for H_{UPD}. This result is similar to those of Sn/Pd electrodes [35]. LSVs of Pd(100) and Sn/Pd(100) electrodes for the NO_3RR were recorded in 0.1 M $HClO_4$ (Fig. 1b). The unmodified Pd(100) electrode had no nitrate reduction activity because there is almost no difference of LSVs of Pd(100) in the presence and absence of nitrate. In contrast, reduction currents with an onset potential of about 0.35 V vs. RHE were observed in the LSV of Sn/Pd(100) in the presence of nitrate, which was attributed to the reduction of nitrate.

The nitrate reduction activity of the Sn/Pd(100) electrode depends on the pH value of the electrolyte solution. The cathodic currents for the nitrate reduction decreased as the pH value increased (Fig. 1c). The relationship between pH and nitrate reduction current was obtained referring to the current density values of the LSV curves at 0.3 V vs. RHE (Fig. 1d). It is worth noting that θ_{Sn} also holds the potential to contribute to fluctuations in NO_3RR current density. Yet, achieving quantitative control over θ_{Sn} during the preparation of Sn/Pd(100) using the immersion process proves challenging. What is certain is that at the potential of 0.3 V vs. RHE, with a nitrate concentration of 10 mM, and under the same pH conditions, the change in NO_3RR current density of Sn/Pd(100) caused by θ_{Sn} can be limited to within 1 mA/cm² [19][35]. Consequently, Fig. 1d can be interpreted as representing changes in NO_3RR activity

predominantly driven by pH levels.

Overall, the nitrate reduction current decreased slowly in the pH range of 1 to 2, while decreased rapidly in the pH range of 2 to 4. When the pH exceeded 4, there was almost no nitrate reduction current can be observed. The curve fitting analysis gives an inflection point at about pH 2.6. This indicates that structural changes of tin species or protonation/deprotonation of nitrate or tin species occur at this pH and would be critical to showing the nitrate reduction activity for Sn/Pd(100). More details on the origin of this pH effect are discussed in the following section based on results of DFT calculation.

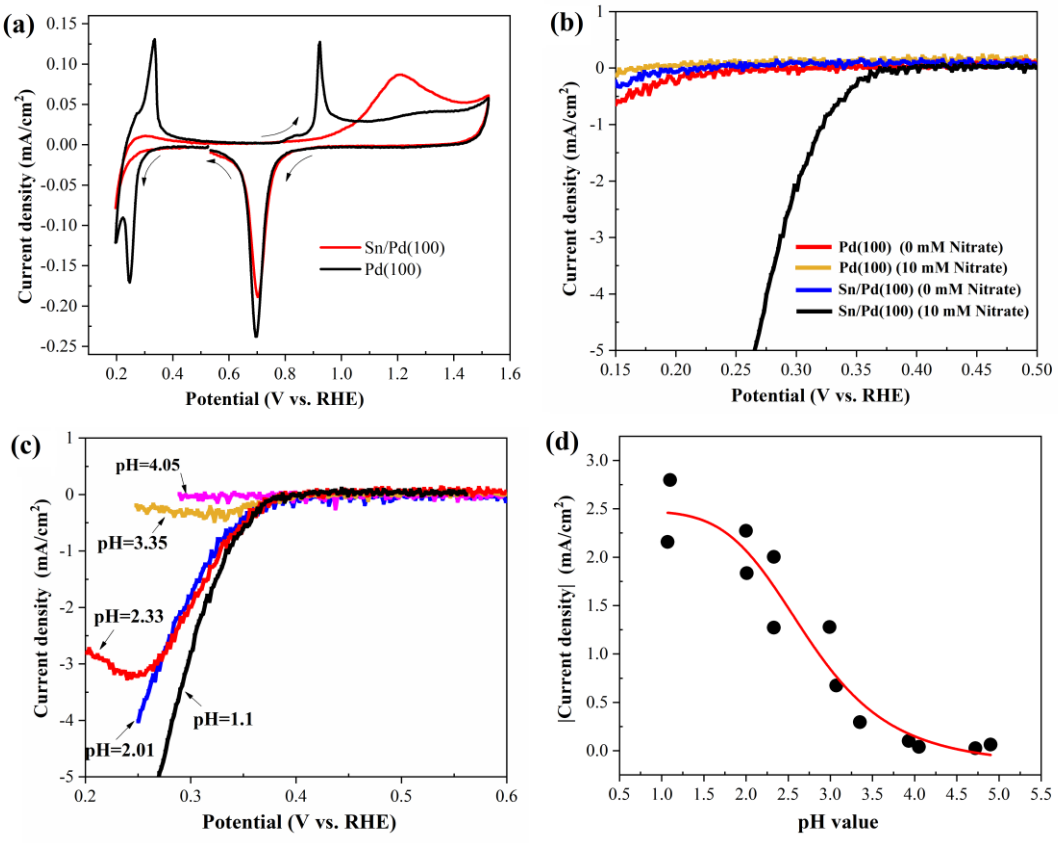

Fig. 1. (a) CVs of Pd(100) (the trace in black) and Sn/Pd(100) (the trace in red). Experimental condition: 0.5 M H_2SO_4; sweep rate: 20 mV/s; θ_{Sn} = 78.8%. (b) LSVs of Pd(100) and Sn/Pd(100) for the nitrate reduction reaction. The LSVs of Pd(100) recorded in 0.1 M $HClO_4$ containing 0 mM and 10

mM sodium nitrate at pH 1.04 and 1.13 under Ar, respectively. The LSVs of Sn/Pd(100) with θ_{Sn} of 61.7 and 80.6% recorded in 0.1 M $HClO_4$ containing 0 and 10 mM sodium nitrate at pH 1.11 and 1.07 under Ar, respectively. All LSVs were recorded at 20 mV/s. (c) Representative LSVs of Sn/Pd(100) recorded in 0.1 M $HClO_4$ containing 10 mM sodium nitrate at different pH values under Ar. (d) The relationship between pH values and current densities of Sn/Pd(100) at 0.3 V vs. RHE for the nitrate reduction reaction. The experimental conditions are shown in Table S1.

3.2. Effects of Sn structures on nitrate reduction under different pH value

3.2.1 Nitrate adsorption capacity of Sn sites

The structural change of Sn species at different pH can affect the nitrate reduction activity of the Sn/Pd(100) electrode. Previously reported X-ray photoelectron spectroscopy (XPS) results confirmed that Sn^{2+} species were mainly found in Sn-modified Pd or Pd-Pt electrodes [18, 36, 37]. The existing form of stannous ions (Sn^{2+}) at different pH values can be predicted by Pourbaix diagram [38-39]: Sn^{2+} are stable at pH < 3.8; $Sn(OH)^+$ can be found at 3.8 < pH < 4; and $Sn(OH)_2$ can be dominant at pH > 4 [40].

It had been confirmed that the initial steps of nitrate reduction include: i) the adsorption process of nitrate at the active site (Eq. 8) [41]; ii) Electron injection into the nitrate molecule (Eq. 9) [42]; iii) Removal of an oxygen atom from the nitrate molecule by electrophilic attack of H^+ (Eq. 10) [43].

$$NO_3^- \rightarrow NO_3^-{}_{(ad)} \quad (8)$$

$$NO_3^-{}_{(ad)} + e^- \rightarrow NO_3^{2-}{}_{(ad)} \quad (9)$$

$$NO_3^{2-}{}_{(ad)} + 2H^+ + e^- \rightarrow NO_2^-{}_{(ad)} + H_2O \quad (10)$$

To understand the pH effect of the Sn atomic site change on the nitrate reduction reaction at Sn/Pd (100) electrode, the changes of Gibbs free energy (ΔG) of the nitrate adsorption on Pd(100), single Sn atom, and Sn/Pd(100) with different Sn species of Sn^{2+}, $Sn(OH)^{+}$, and $Sn(OH)_2$ were calculated by density functional theory (DFT) (Fig. 2). Pd(100) without Sn modification shows the rise of ΔG during the nitrate adsorption process, indicating that the process was not spontaneous. This result is in good agreement with the experimental result of the Pd(100) electrode for the nitrate reduction reaction (Fig. 1b) and previously reported calculations of ΔG of the nitrate adsorption to Pd [31]. In contrast, a strong nitrate adsorption occurs to the single Sn atom with ΔG of -2.57 eV. Therefore, the nitrate adsorption, which is the first step of the nitrate reduction processes, occurs at the Sn site [44].

A ΔG value for the nitrate adsorption on Sn^{2+}/Pd(100) was calculated to be -0.15 eV. Although it was higher than that of the nitrate adsorption process at the single Sn atom, the modification of Sn^{2+} promotes the adsorption of nitrate on the surface of Sn/Pd(100) thermodynamically. The energy comparison between N- and O-bonded nitrate to Sn^{2+} also reveals that the Sn-O formation between nitrate and Sn^{2+} is more favorable on Sn/Pd(100) (Fig. 2c). In our DFT calculation, $Sn(OH)^{+}$/Pd(100) and $Sn(OH)_2$/Pd(100) have no nitrate adsorption capacity for Sn/Pd(100), which have the increasing ΔG value for the nitrate adsorption of 0.22 and 0.39 eV (Fig. 2d and Fig. 2e), respectively. The above results were attributed to the formation of Sn-O bond by the bonding between OH^- and Sn atom deprived the Sn 2p orbital electrons that

supported the bonding between NO_3^- and Sn atom at the low energy level, thus it was difficult for nitrate to bond with Sn 2p orbital electrons. This part was discussed in detail in section 3.2.2. Since $Sn(OH)^+$ and $Sn(OH)_2$ is dominant at pH > 3.8, almost no current of the Sn/Pd(100) electrode for the nitrate reduction reaction was detected (Fig. 1c and Fig. 1d).

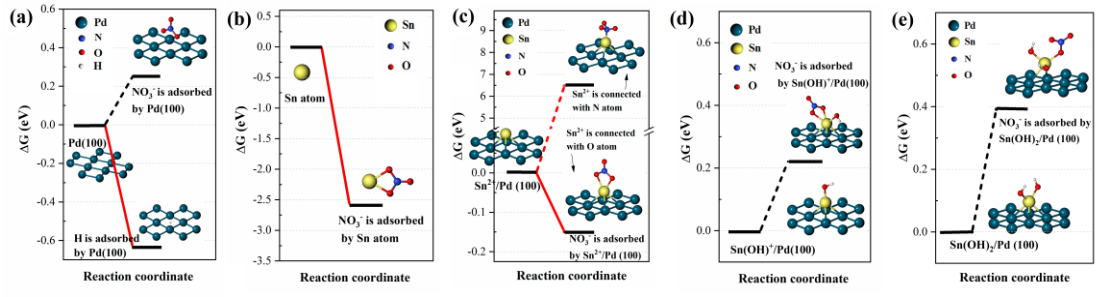

Fig. 2 The changes of Gibbs free energy (ΔG) during NO_3^- adsorption on Pd(100) (a), Sn atom (Sn^0) (b), Sn^{2+}/Pd(100) (c), $Sn(OH)^+$/Pd(100) (d), and $Sn(OH)_2$/Pd(100) (e) at 0 V vs. RHE.

3.2.2 Electron affinity of nitrate adsorbed on Sn sites

According to the results of structural optimization, Sn atom seemed to be repulsive to N atom, but attractive to O atom, which meant that the formation of Sn-O bond can weaken N–O bonding in the NO_3^- molecule. Similar results had been observed in a previous report on Sn-Pt materials that Sn changed the local electron density of its bonding atoms, and then affecting the coulomb force between the bonding atoms and other atoms [45]. The binding of nitrate to Sn sites should also change the molecular orbitals of nitrate molecules.

In this viewpoint, the lowest unoccupied molecular orbital (LUMO) energies of

316 nitrate molecules after binding to different Sn sites were explored by density of states
317 (DOS) analysis (Fig. 3). For the nitrate reduction, the injection of electrons into the
318 anti-bonding molecular orbital of N–O is necessary to break N–O bonding and the
319 LUMO is placed at about 2.3 eV (Fig. 3a). The result of high electron injection energy
320 barrier of nitrate molecule was also mentioned in the study of da Cunha and
321 co-workers [46]. The LUMO energies of nitrate were reduced to 1.3 eV and 2.0 eV
322 after the adsorption to a single Sn atom (Fig. 3b) and Pd(100) (Fig. 3c), respectively.
323 Both Sn atom and Pd atom contribute to reducing the LUMO energy of nitrate and
324 promoting electron injection. Because the Sn atomic site more significantly reduce the
325 nitrate reduction barrier than the Pd atomic site, Sn atom is the main active site for the
326 NO_3RR.

327 The partial density of states (PDOS) of 2p orbital shown that in Sn^0 the 2p orbital
328 electron of Sn atom near 1.3 eV can effectively form a covalent bond with the 2p
329 orbital electron of O atom in nitrate molecule (Fig. 4a). Sn^{2+} in Sn^{2+}/Pd(100) can also
330 form a bond with nitrate molecule near 1.5 eV, and achieved the decreasing LUMO
331 energy for nitrate molecule (Fig. 3d and Fig. 4b). Therefore, in the range of pH < 3.8,
332 Sn/Pd(100) electrode can effectively adsorb nitrate molecule and reduce the LUMO
333 energy of nitrate molecules, which promoted electron injection into nitrate molecule
334 and nitrate reduction.

335 On the other hand, when nitrate was connected with $Sn(OH)^+$/Pd(100) and
336 $Sn(OH)_2$/Pd(100), LUMO energy of nitrate molecule was increased to 2.7 and 2.8 eV,

respectively (Fig. 3e and Fig. 3f). This phenomenon can be easily understood through the PDOS calculation results of 2p orbital. During the formation of $Sn(OH)^+$/Pd(100) or $Sn(OH)_2$/Pd(100), the electrons of O atom in OH^- mainly overlapped with 2p orbital electrons in Sn atom near 1.3 eV to form Sn-O bond (Fig. 4c and Fig. 4d). Thus the binding of nitrate based on $Sn(OH)^+$/Pd(100) or $Sn(OH)_2$/Pd(100) mainly through the 2p orbital electrons of Sn atoms near 2.5 eV. This meant that in the above case, the formation of Sn-O bond will raise the LUMO energy of nitrate molecule. Therefore, Sn/Pd(100) was difficult to achieve effective electron injection into nitrate molecules when pH > 3.8, and loss nitrate reduction activity.

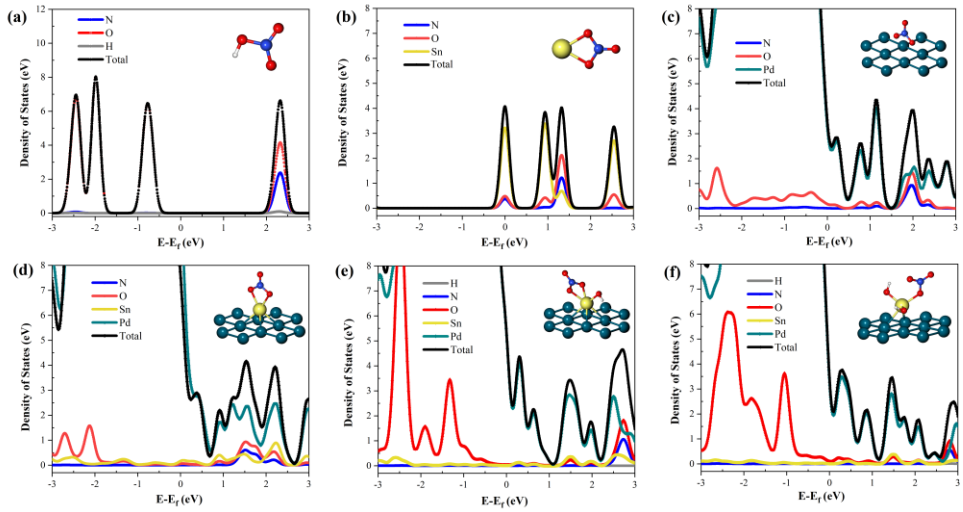

Fig. 3 Density of states (DOS) diagram of different structures. (a) nitric acid; (b) nitrate combination with Sn^0; (c) nitrate combination with Pd(100); (d) nitrate combination with Sn^{2+}/Pd(100); (e) nitrate combination with $Sn(OH)^+$/Pd(100); (f) nitrate combination with $Sn(OH)_2$/Pd(100).(E_f is the Fermi energy)

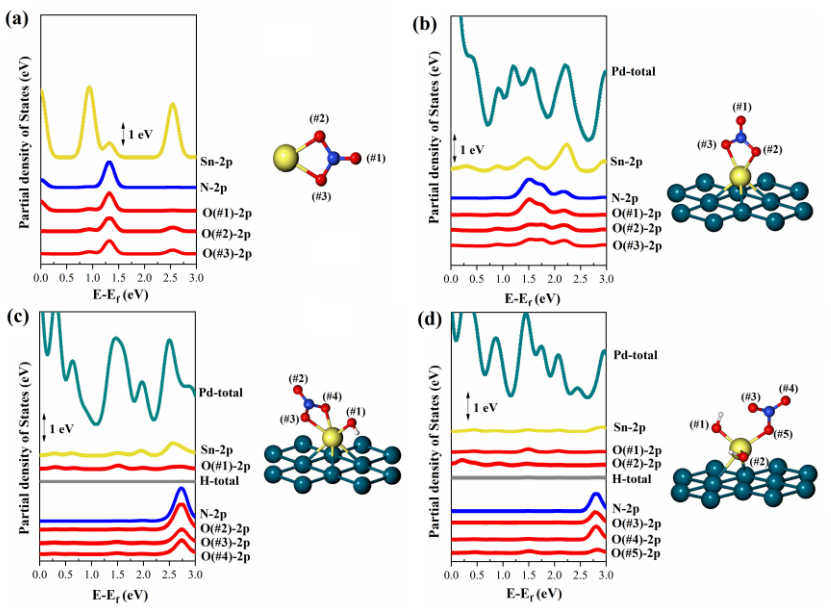

Fig. 4 Partial density of states (PDOS) diagram of different structures. (a) nitrate combination with Sn^0; (b) nitrate combination with Sn^{2+}/Pd(100); (c) nitrate combination with $Sn(OH)^+$/Pd(100); (d) nitrate combination with $Sn(OH)_2$/Pd(100). (E_f is the Fermi energy)

3.2.3 Electrophilic reactivity of nitrate molecule after connected with Sn sites

In this study, the electrostatic potential (ESP) of nitrate and nitrate adsorbed by Sn/Pd(100) was calculated to further explore the influence of adsorption process on nitrate. The ESP at the point coordinate ***r*** can be calculated by Eq. 11 [47]

$$ESP = V(r) = \sum_A \frac{Z_A}{|R_A - r|} - \int \frac{\rho(r')dr'}{|r' - r|} \quad (11)$$

where A is the type of nucleus in the molecule, Z is the number of nuclear charges. R_A and $\boldsymbol{r}'$ is the coordinate of the nucleus and extranuclear electrons, respectively. The averaged electron number in each volume element $d\boldsymbol{r}$ is given by the electronic density function ($\rho(r)$). $|R_A - \boldsymbol{r}|$ represents the distance between nucleus and the point ***r***, just as $|\boldsymbol{r}' - \boldsymbol{r}|$ is the distance between each extranuclear electron and the point ***r***. ESP

366 indicates the total electrostatic interaction energy between a unit positive charge at the
367 point coordinate ***r*** and system (nucleus and extranuclear electrons).

368 The van der Waals surface is defined as an isosurface with an ρ(r) of 0.001 e/Bohr^3
369 [48]. This can provide a measure of electrophilic / nucleophilic attacks between
370 molecules [49]. Generally, the more negative the ESP is, the more likely it is to react
371 with the positively charged species like H^+ [50]. The ESP of O atoms in nitrate
372 molecule decreases significantly after binding with a single Sn atom (Fig. 5a and Fig.
373 b), which can be attributed to the increase of the number of electrons near O atoms by
374 the overlap of Sn and O orbital after Sn-O bonding. In addition, when nitrate molecule
375 was directly connected to Pd(100), the ESP of O atoms in nitrate also decreased
376 significantly (Fig. 5c), which means that there is also orbital overlap between Pd atom
377 and O atom. Because of both Sn and Pd atoms are beneficial to reduce the ESP of O
378 atom in the nitrate molecule, the adsorption of nitrate to Sn/Pd(100) promotes the
379 electrophilic attack of H^+ on nitrate molecule, that is, promotes Eq. 10 during
380 electrolysis.

381 Moreover, although the ESPs of all O atoms in the nitrate molecule were decreased
382 significantly after the adsorption on Sn/Pd(100) , the lowest ESP was obtained at the
383 O atom that has the farthest distance from the binding site (Fig. 5d). Therefore, during
384 the process of H^+ based electrophilic reaction, the farthest O atom can be protonated
385 first.

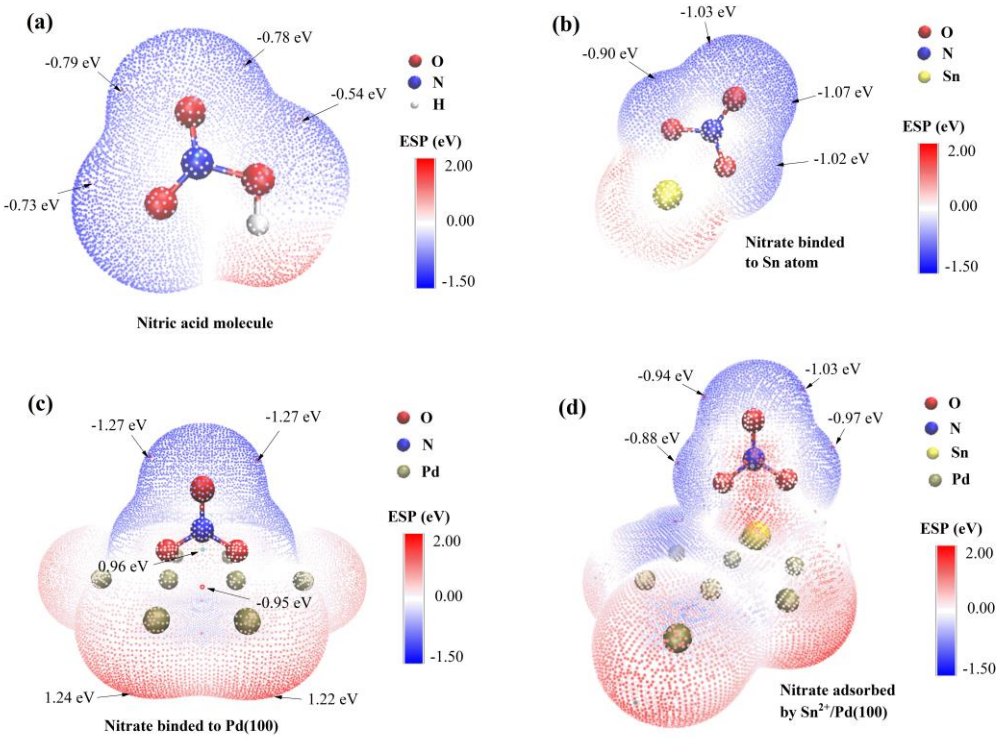

386

387 **Fig. 5** (a) The electrostatic potential (ESP) of nitric acid molecule; (b) The ESP of nitrate absorbed by
388 single Sn atom; (c) The ESP of nitrate binded to Pd(100); (d) The ESP of nitrate absorbed by
389 Sn/Pd(100).

390 In summary, Sn/Pd(100) shows the nitrate reduction activity at pH < 3.8, where
391 Sn^{2+} can be involved in the adsorption of nitrate on the Sn/Pd(100) electrode. The
392 LUMO energy of nitrate can be decreased by the adsorption on Sn and Pd atoms. The
393 nitrate adsorption process also reduced the ESP of O atoms in the nitrate molecule,
394 which was advantageous to the protonation of nitrate.

395

396 **3.3. Effect of pH on the nitrite (NO_2^-) reduction reaction catalyzed at Pd(100)**

397 Although results of DFT calculations indicate that the nitrate reduction reaction can
398 be catalyzed at the Sn/Pd(100) electrode at pH < 3.8, the decrease of the cathodic

currents is observed even at pH < 3.8 (Fig. 1d). To further explore the continuous reduction process for the nitrate reduction reaction, the nitrite reduction reaction at Pd(100) was studied. For the nitrite reduction reaction, Pd itself works as an active site [51-52]. It is necessary to further confirm which is the main active site for the nitrite reduction, the Sn or Pd site.

Fig. 6a shows linear sweep voltammograms of the Pd(100) electrode for the nitrite reduction at different pH values. A peak was observed with onset and peak potentials at about 0.6 and 0.4 V vs. RHE, respectively. Moreover, at pH lower than 2.58, the formation of reduction current can also be observed near the electrode potential of 0.1 V vs. RHE. The above results were consistent with the previous observation of nitrite reduction in 0.1 M $HClO_4$ using Pd electrode [51]. The pH dependence of CV curves of the Sn/Pd (100) electrode was basically the same as that of the Pd(100) electrode without Sn modification (Fig. S1). This phenomenon means that Sn modification plays no significant role in the nitrate reduction and the nitrite reduction mainly occurs at the Pd atomic site. This result was also consistent with the previous observation that Sn modification had almost no effect on the electrochemical reduction of nitrite by Pd electrode in 0.1 M $HClO_4$ [51]. The thermodynamic results of the nitrite reduction obtained from DFT calculations also support the experimental results: the nitrite reduction at the Sn atomic site on the surface of Sn^{2+}/Pd(100) gave a positive ΔG value. Thus, the reduction of nitrite occurs at the Pd atomic site (Fig. 6b). In this study, we mainly focused on the reduction behavior of nitrite at Pd atomic

site.

The nitrite reduction current densities of Pd(100) at 0.1 and 0.4 V vs. RHE at different pH were extracted and then plotted as the pH dependence curve, as shown in Fig. 6c-6d. Almost no current densities were observed at higher pH values than the p*K*a value of HNO_2 (3.25). At pH < p*K*a (HNO_2), HNO_2 is dominant in solution while NO_2^- at pH > p*K*a (HNO_2) (Eq. 12).

$$NO_2^- + H^+ \rightleftharpoons HNO_2 \qquad (pKa = 3.25) \qquad (12)$$

Previous study has shown that the direct reduction of NO_2^- by Pd electrode is difficult which depends on the chemical reaction between adsorbed species (Pd-H and Pd-NO_2^-) formed at Pd atomic sites [53]. More importantly, the formation of Pd-NO_2^- was also limited by the competition of Pd-H, makes the Pd-NO_2^- difficult to be formed [53]. Thus, the formation of HNO_2 seems very important to mediate the continuous reduction of nitrite on the surface of Pd (100) according to Fig. 6c-6d.

To understand the nitrite reduction mechanism, we should consider the disproportionation of HNO_2 under acidic conditions. Previous studies had confirmed that HNO_2 was unstable under acidic conditions and promoted the formation of NO (Eq. 13) [54-55].

$$2HNO_2 \rightleftharpoons NO + NO_2 + H_2O \qquad (13)$$

NO can quickly adsorb at Pd atoms on the Sn/Pd(100) surface (Eq. 14).

$$NO + Pd^* \rightarrow Pd^*NO \qquad (14)$$

This process can be confirmed by DFT calculations in this study: Δ*G* of NO

adsorbed by Pd atoms (-2.29 eV) was much lower than that of H^+ (-0.63 eV). These results were also consistent with previous results of FTIR studies on the NO adsorption on the surface of Pd atoms [56].

Moreover, the direct reduction of HNO_2 can also promote the formation of adsorbed NO (Eq. 15) [57].

$$HNO_2 + H^+ + e^- \rightarrow NO_{ads} + H_2O \quad (15)$$

After the formation of the adsorbed NO, it can react with HNO_2 in solution and then N_2O is produced (Eq. 16) [57]. These processes can occur in the potential range between 0.3 and 0.5 V vs. RHE [21]. Therefore, the peak at about 0.4 V vs. RHE for the nitrite reduction (Fig. 6a) can be attributed to the process of Eqs. 14-16 and finally promote the formation of N_2O.

$$HNO_{2,aq} + NO_{ads} + 3H^+ + 3e^- \rightarrow N_2O + 2H_2O \quad (16)$$

The above discussion also can be confirmed from our previous results of differential electrochemical mass spectrometry (DEMS) that N_2O was dominant in the gaseous products of nitrate reduction by Sn/Pd (100) electrode (0.2 V vs. RHE) [19]. Cathodic currents at 0.1 V vs. RHE can be attributed to the conversion of HNO_2 to NH_3OH^+ (Eq. 17) [58].

$$HNO_2 + 5H^+ + 4e^- \rightarrow NH_3OH^+ + H_2O \quad (17)$$

From a kinetic point of view, Eq. 17 highly depends on the concentration of H^+ rather than Eqs. 15-16. Therefore, compared with the cathodic currents near 0.4 V vs. RHE, the cathodic currents near 0.1 V vs. RHE decrease more quickly as pH values

increase (Fig. 6c).

In conclusion, since the occurrence of Eqs. 13-17 depended on the formation of HNO_2, the dissociation of intermediate nitrite was the main reason for the decreasing nitrite reduction current of Pd(100) electrode with the increasing pH value in the range of pH < 3.8. This also means that adjusting the suitable pH value to control the degree of protonation of nitrite in intermediate products would be very important to maximize the nitrate reduction efficiency to design or develop practical electrocatalytic systems in the future.

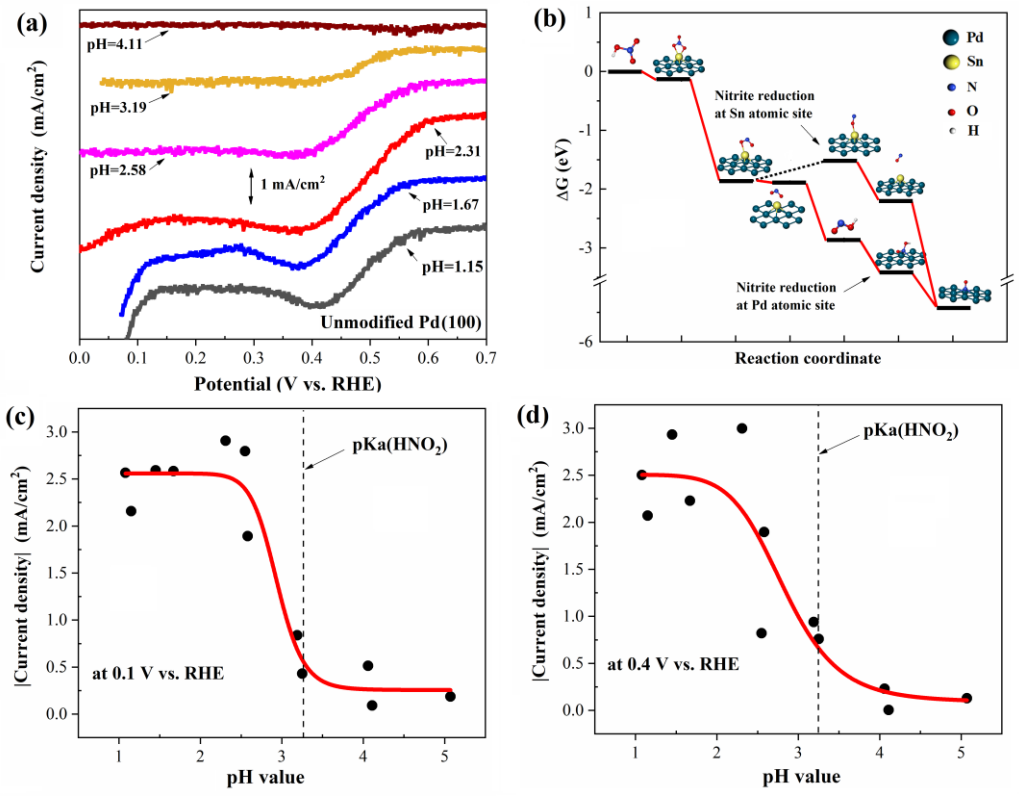

Fig. 6 (a) the nitrite reduction behavior of Pd(100) under different pH values; (b) the Gibbs free energy change of nitrite reduction at Sn atomic site and Pd atomic site (0 V vs. RHE); (c) the current values of nitrite reduction by Pd(100) at 0.1 V vs. RHE under different pH value; (d) the current values of nitrite reduction by Pd(100) at 0.4 V vs. RHE under different pH value. The experimental conditions for Fig. 6(a), 6(c), and 6(d) were provided in Table S2.

3.4. Mechanism analysis

Based on the results of this study, the effect mechanism of pH on Sn/Pd(100) for nitrate reduction can be described as follows (Fig. 7):

(i) pH < pKa (HNO_2) = 3.25

The adsorption and reduction processes of NO_3^- at Sn atomic site were remarkable. The intermediate product of HNO_2 mediated its decomposition on Pd surface and promote the formation of N_2O and NH_3OH^+. The nitrate reduction current was decreased with the decreasing percentage of intermediate HNO_2 controlled by pH.

(ii) pKa(HNO_2) = 3.25 < pH < 3.8

The conversion from NO_3^- to NO_2^- on the electrode surface can be occurred. The deprotonation of HNO_2 lead to the decreasing of overall nitrate reduction current.

(iii) pH > 3.8

The Sn site is evolved into $Sn(OH)^+$ or $Sn(OH)_2$, which lost the adsorption capacity of NO_3^-, and the electrode activity disappeared.

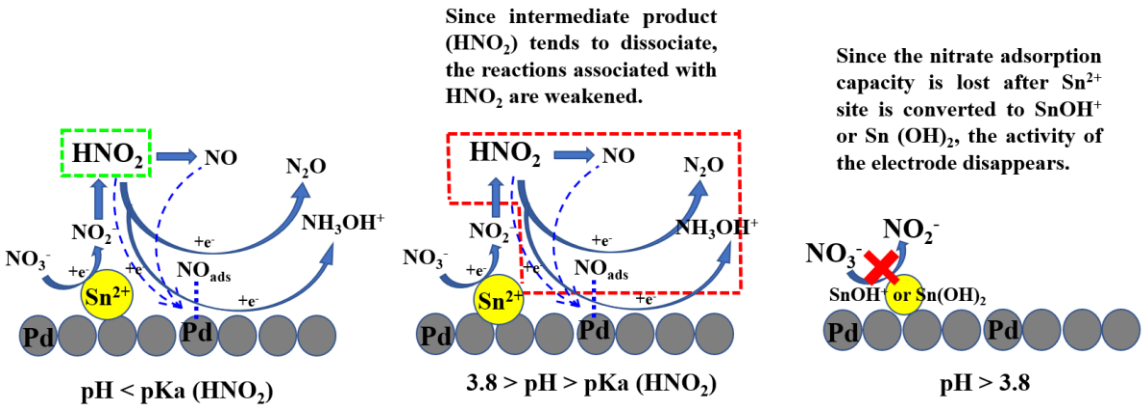

Fig.7. The mechanism of different pH values on the activity of Sn/Pd(100) for nitrate reduction

4. Conclusions

In this study, the effect of pH value for the nitrate reduction by the Sn/Pd(100) electrode was evaluated. At <pH 3.8, the Sn/Pd(100) electrode had nitrate reduction activity with Sn atomic sites in the form of Sn^{2+}, where (i) Sn atomic sites promoted nitrate adsorption; (ii) the combined action of Sn and Pd atoms can reduce the energy level of the LUMO of the nitrate molecule and the van der Waals electrostatic potential of the O-N bond, which promoted electron injection into nitrate as well as protonation to nitrate. At >pH 3.8, the formation of $Sn(OH)^+$ or $Sn(OH)_2$ inhibits the adsorption of NO_3^- on Sn atoms, resulting in no electrocatalytic activity for the NO_3RR. Sn atom sites mainly support the reduction step of NO_3^- to NO_2^-, and the subsequent continuous reduction mainly occur on Pd atom sites. The protonation of NO_2^- is crucial to the nitrite reduction on Pd(100) surface and therefore the deprotonation of HNO_2 reduces the overall current density for the nitrite reduction. The findings in this study will encourage us to understand the nitrate reduction mechanism at Sn/Pd electrodes and develop novel approaches or substrate materials, specifically those capable of safeguarding and sustaining Sn^{2+} on the electrode's surface, which is critical for efficient NO_3RR performance in applications.

Acknowledgements

The authors thank Takao Ohta (Graduate School of Engineering, Hokkaido University), Katsuhisa Ishikawa and Takahiko Hasegawa (Technical Division, Institute for Catalysis, Hokkaido University) for their technical support on electrochemical glassware. This work was supported by China Scholarship Council (to Yang Deng) for his visiting research in Hokkaido University and JSPS KAKENHI Grant numbers JP16K20882, JP21K05124 (to MK), and JP19H02664 (to IY).

Credit Author Statement

Yang Deng: Conceptualization, Methodology, Validation, Investigation, Formal analysis, Writing-original draft, Software, Writing - review and editing.

Masaru Kato: Conceptualization, Supervision, Methodology, Formal analysis, Writing - review and editing.

Jinhang Zheng: Methodology, Writing - review and editing.

Chuanping Feng: Methodology, Writing - review and editing.

Ichizo Yagi: Conceptualization, Supervision, Methodology, Formal analysis, Project administration, Writing - review and editing.

References

[1] S.A. Wherry, A.J. Tesoriero, S. Terziotti, Factors Affecting Nitrate Concentrations in Stream Base Flow, Environ. Sci. Technol. 55 (2021) 902–911.

[2] Y. Sun, M. Nemati, Evaluation of sulfur-based autotrophic denitrification and denitritation for biological removal of nitrate and nitrite from contaminated waters, Bioresour. Technol. 114 (2012) 207–216.

[3] Y. Deng, N. Chen, C. Feng, H. Wang, Y. Zheng, F. Chen, W. Lu, P. Kuang, H. Feng, Y. Gao, W. Hu, Degradation of nitrogen-containing refractory organic wastewater using a novel alternating-anode electrochemical system, Sci. Total Environ. 697 (2019) 134161.

[4] H. Özen, U. Kamber, M. Karaman, S. Gül, E. Atakişi, K. Özcan, O. Atakişi, Histopathologic, biochemical and genotoxic investigations on chronic sodium nitrite toxicity in mice, Exp. Toxicol. Pathol. 66 (2014) 367–375.

[5] USEPA, US. Environmental Protection Agency–USEPA. 2012.Endocrine Disruptor Screening Program, Universe of Chemicals for Potential Endocrine Disruptor Screening and Testing., 2012.

[6] P. Kuang, C. Feng, N. Chen, W. Hu, G. Wang, T. Peng, L. Lv, Improvement on Electrochemical Nitrate Removal by Combining with the Three-Dimensional (3-D) Perforated Iron Cathode and the Iron Net Introduction, J. Electrochem. Soc. 163 (2016) E397–E406.

[7] B.P. Dash, S. Chaudhari, Electrochemical denitrificaton of simulated ground water, Water Res. 39 (2005) 4065–4072.

[8] D. Takaoka, M. Ikematsu, M. Iseki, K. Takizawa, S. Kawata, Removal of nitrogen and phosphorus by electrolysis using a pair of iron electrodes, Electrochem. -Tokyo-. 72 (2004) 27–31.

[9] M. Li, C. Feng, Z. Zhang, S. Yang, N. Sugiura, Treatment of nitrate contaminated water using an electrochemical method, Bioresour. Technol. 101 (2010) 6553–6557.

[10] M. Li, C. Feng, Z. Zhang, N. Sugiura, Efficient electrochemical reduction of nitrate to nitrogen using Ti/IrO_2–Pt anode and different cathodes, Electrochimica Acta. 54 (2009) 4600–4606.

[11] M. Li, C. Feng, Z. Zhang, Z. Shen, N. Sugiura, Electrochemical reduction of nitrate using various anodes and a Cu/Zn cathode, Electrochem. Commun. 11 (2009) 1853–1856.
[12] D. Reyter, D. Bélanger, L. Roué, Optimization of the cathode material for nitrate removal by a paired electrolysis process, J. Hazard. Mater. 192 (2011) 507–513.
[13] T. Zheng, B. Lu, G. Harle, D. Yang, C. Wang, Y. Zhao, A comparative study of Rh-only, Pd-only and Pd/Rh catalysts, Appl. Catal. Gen. 602 (2020) 117649.
[14] P. Kuang, K. Natsui, Y. Einaga, C. Feng, Y. Cui, W. Zhang, Y. Deng, Annealing enhancement in stability and performance of copper modified boron-doped diamond (Cu-BDD) electrode for electrochemical nitrate reduction, Diam. Relat. Mater. 114 (2021) 108310.
[15] P. Kuang, K. Natsui, C. Feng, Y. Einaga, Electrochemical reduction of nitrate on boron-doped diamond electrodes: Effects of surface termination and boron-doping level, Chemosphere. 251 (2020) 126364.
[16] J. Souza-Garcia, E.A. Ticianelli, V. Climent, J.M. Feliu, Nitrate reduction on Pt single crystals with Pd multilayer, Electrochimica Acta. 54 (2009) 2094–2101.
[17] Y.Y. Birdja, J. Yang, M.T.M. Koper, Electrocatalytic Reduction of Nitrate on Tin-modified Palladium Electrodes, Electrochimica Acta. 140 (2014) 518–524.
[18] M. Kato, M. Okui, S. Taguchi, I. Yagi, Electrocatalytic nitrate reduction on well-defined surfaces of tin-modified platinum, palladium and platinum-palladium single crystalline electrodes in acidic and neutral media, J. Electroanal. Chem. 800 (2017) 46-53.
[19] M. Kato, Y. Unuma, M. Okui, Y. Qu, J. Zheng, S. Taguchi, F. Kiguchi, M. Torihata, Y. Gao, N. Hoshi, I. Yagi, Electrocatalytic activity and volatile product selectivity for nitrate reduction at tin-modified Pt(100), Pd(100) and Pd–Pt(100) single crystal electrodes in acidic media, Electrochimica Acta. 398 (2021) 139281.
[20] K. Shimazu, R. Goto, K. Tada, Electrochemical Reduction of Nitrate Ions on Tin-Modified Platinum and Palladium Electrodes, Chem. Lett. 31 (2002) 204–205.
[21] M. Duca, V. Kavvadia, P. Rodriguez, S.C.S. Lai, T. Hoogenboom, M.T.M. Koper, New insights into the mechanism of nitrite reduction on a platinum electrode, J. Electroanal. Chem. 649 (2010) 59–68.
[22] N. Hoshi, K. Kida, M. Nakamura, M. Nakada, K. Osada, Structural Effects of Electrochemical Oxidation of Formic Acid on Single Crystal Electrodes of Palladium, J. Phys. Chem. B. 110 (2006) 12480–12484.
[23] R.W.G. Wyckoff, Crystal Structures, New York, New York, 1963.
[24] P. Giannozzi, S. Baroni, N. Bonini, M. Calandra, R. Car, C. Cavazzoni, D. Ceresoli, G.L. Chiarotti, M. Cococcioni, I. Dabo, A. Dal Corso, S. de Gironcoli, S. Fabris, G. Fratesi, R. Gebauer, U. Gerstmann, C. Gougoussis, A. Kokalj, M. Lazzeri, L. Martin-Samos, N. Marzari, F. Mauri, R. Mazzarello, S. Paolini, A. Pasquarello, L. Paulatto, C. Sbraccia, S. Scandolo, G. Sclauzero, A.P. Seitsonen, A. Smogunov, P. Umari, R.M. Wentzcovitch, QUANTUM ESPRESSO: a modular and open-source software project for quantum simulations of materials, J. Phys. Condens. Matter Inst. Phys. J. 21 (2009) 395502.
[25] K. Lejaeghere, G. Bihlmayer, T. Björkman, P. Blaha, S. Blügel, V. Blum, D. Caliste, I.E. Castelli, S.J. Clark, A.D. Corso, S. de Gironcoli, T. Deutsch, J.K. Dewhurst, I.D. Marco, C. Draxl, M. Dułak, O. Eriksson, J.A. Flores-Livas, K.F. Garrity, L. Genovese, P. Giannozzi, M.

Giantomassi, S. Goedecker, X. Gonze, O. Grånäs, E.K.U. Gross, A. Gulans, F. Gygi, D.R. Hamann, P.J. Hasnip, N. a. W. Holzwarth, D. Iuşan, D.B. Jochym, F. Jollet, D. Jones, G. Kresse, K. Koepernik, E. Küçükbenli, Y.O. Kvashnin, I.L.M. Locht, S. Lubeck, M. Marsman, N. Marzari, U. Nitzsche, L. Nordström, T. Ozaki, L. Paulatto, C.J. Pickard, W. Poelmans, M.I.J. Probert, K. Refson, M. Richter, G.-M. Rignanese, S. Saha, M. Scheffler, M. Schlipf, K. Schwarz, S. Sharma, F. Tavazza, P. Thunström, A. Tkatchenko, M. Torrent, D. Vanderbilt, M.J. van Setten, V.V. Speybroeck, J.M. Wills, J.R. Yates, G.-X. Zhang, S. Cottenier, Reproducibility in density functional theory calculations of solids, Science. 351 (2016) 6280.

[26] G. Prandini, A. Marrazzo, I.E. Castelli, N. Mounet, N. Marzari, Precision and efficiency in solid-state pseudopotential calculations, Npj Comput. Mater. 4 (2018) 1–13.

[27] J. Wang, L. Yu, L. Hu, G. Chen, H. Xin, X. Feng, Ambient ammonia synthesis via palladium-catalyzed electrohydrogenation of dinitrogen at low overpotential, Nat. Commun. 9 (2018) 1795.

[28] G. Li, Y. Yu, Z. Pan, L. An, Two-Dimensional Layered SnO2 Nanosheets for Ambient Ammonia Synthesis, ACS Appl. Energy Mater. 3 (2020) 6735–6742.

[29] F. Neese, Software update: the ORCA program system, version 4.0, WIREs Comput. Mol. Sci. 8 (2018) e1327.

[30] T. Lu, F. Chen, Multiwfn: A multifunctional wavefunction analyzer, J. Comput. Chem. 33 (2012) 580–592.

[31] J.-X. Liu, D. Richards, N. Singh, B.R. Goldsmith, Activity and Selectivity Trends in Electrocatalytic Nitrate Reduction on Transition Metals, ACS Catal. 9 (2019) 7052–7064.

[32] F. Calle-Vallejo, M. Huang, J.B. Henry, M.T.M. Koper, A.S. Bandarenka, Theoretical design and experimental implementation of Ag/Au electrodes for the electrochemical reduction of nitrate, Phys. Chem. Chem. Phys. 15 (2013) 3196–3202.

[33] J.J. Fifen, Thermodynamics of the Electron Revisited and Generalized | Journal of Chemical Theory and Computation, J Chem Theory Comput. 9 (2013) 3165–3169.

[34] W. Beckon, C. Parkins, A. Maximovich, A. Beckon. A General Approach to Modeling Biphasic Relationships, Environ. Sci. Technol. 42 (2008) 1308–1314.

[35] Md. Motahar Hossain, K. Nakata, T. Kawaguchi, K. Shimazu, Reduction of nitrate on electrochemically pre-reduced tin-modified palladium electrodes, J. Electroanal. Chem. 707 (2013) 59–65.

[36] M. Hossain, T. Kawaguchi, K. Shimazu, K. Nakata, Reduction of nitrate on tin-modified palladium-platinum electrodes, J. Electroanal. Chem. 864 (2020) 114041.

[37] M. Hossain, K. Nakata, T. Kawaguchi, K. Shimazu, Reduction of nitrate on electrochemically pre-reduced tin-modified palladium electrodes, J. Electroanal. Chem. 707 (2013) 59–65.

[38] D. Minzari, M.S. Jellesen, P. Møller, R. Ambat, On the electrochemical migration mechanism of tin in electronics, Corros. Sci. 53 (2011) 3366–3379.

[39] W. Sun, D.A. Kitchaev, D. Kramer, G. Ceder, Non-equilibrium crystallization pathways of manganese oxides in aqueous solution, Nat. Commun. 10 (2019) 573.

[40] Y. Nakamaru, S. Uchida, Distribution coefficients of tin in Japanese agricultural soils and the factors affecting tin sorption behavior, J. Environ. Radioact. 99 (2008) 1003–1010.

[41] I. Katsounaros, G. Kyriacou, Influence of the concentration and the nature of the supporting electrolyte on the electrochemical reduction of nitrate on tin cathode, Electrochimica Acta. 52 (2007) 6412–6420.
[42] A.R. Cook, N. Dimitrijevic, B.W. Dreyfus, D. Meisel, L.A. Curtiss, D.M. Camaioni, Reducing Radicals in Nitrate Solutions. The NO_3^{2-} System Revisited, J. Phys. Chem. A. 105 (2001) 3658–3666.
[43] Z. Mumtarin, M.M. Rahman, H.M. Marwani, M.A. Hasnat, Electro-kinetics of conversion of NO3− into NO2−and sensing of nitrate ions via reduction reactions at copper immobilized platinum surface in the neutral medium, Electrochimica Acta. 346 (2020) 135994.
[44] Z.-L. Wu, Y.-J. Shih, Bimetallic palladium-tin nanoclusters, PdSn(200) and PdSn(101), templated with cationic surfactant for electrochemical denitrification toward N_2 and NH_4^+ selectivity, Chem. Eng. J. 433 (2021) 133852.
[45] J.N. Schwämmlein, P.A.L. Torres, H.A. Gasteiger, H.A. El-Sayed, Direct PtSn Alloy Formation by Pt Electrodeposition on Sn Surface, Sci. Rep. 10 (2020) 59.
[46] M.C.P.M. da Cunha, M. Weber, F.C. Nart, On the adsorption and reduction of NO_3^- ions at Au and Pt electrodes studied by in situ FTIR spectroscopy, J. Electroanal. Chem. 414 (1996) 163–170.
[47] J.S. Murray, P. Politzer, The electrostatic potential: an overview, WIREs Comput. Mol. Sci. 1 (2011) 153–163.
[48] R.F.W. Bader, M.T. Carroll, J.R. Cheeseman, C. Chang, Properties of atoms in molecules: atomic volumes, J. Am. Chem. Soc. 109 (1987) 7968–7979.
[49] C. Parlak, M. Akdogan, G. Yildirim, N. Karagoz, E. Budak, C. Terzioglu, Density functional theory study on the identification of 3-[(2-morpholinoethylimino)methyl]benzene-1,2-diol, Spectrochim. Acta. A. Mol. Biomol. Spectrosc. 79 (2011) 263–271.
[50] Y. Tao, X. Li, L. Han, W. Zhang, Z. Liu, Spectroscopy (FT-IR, FT-Raman), hydrogen bonding, electrostatic potential and HOMO-LUMO analysis of tioxolone based on DFT calculations, J. Mol. Struct. 1121 (2016) 188–195.
[51] K. Nakata, Y. Doi, S. Kubota, K. Shimazu, Reduction of nitrite on tin-modified noble metal electrodes, J. Electroanal. Chem. 647 (2010) 187–193.
[52] M. Duca, B. van der Klugt, M.T.M. Koper, Electrocatalytic reduction of nitrite on transition and coinage metals, Electrochimica Acta. 68 (2012) 32–43.
[53] G. Denuault, C. Milhano, D. Pletcher, Mesoporous palladium—the surface electrochemistry of palladium in aqueous sodium hydroxide and the cathodic reduction of nitrite, Phys. Chem. Chem. Phys. 7 (2005) 3545–3551.
[54] P. Wiesen, J. Kleffmann, R. Kurtenbach, K.H. Becker, Mechanistic study of the heterogeneous conversion of NO2 into HONO and N2O on acid surfaces, Faraday Discuss. 100 (1995) 121–127.
[55] K.H. Becker, J. Kleffmann, R. Kurtenbach, P. Wiesen, Solubility of Nitrous Acid (HONO) in Sulfuric Acid Solutions, J. Phys. Chem. 100 (1996) 14984–14990.
[56] B. Álvarez, A. Rodes, J.M. Pérez, J.M. Feliu, J.L. Rodríguez, E. Pastor, Spectroscopic Study of the Nitric Oxide Adlayers Formed from Nitrous Acid Solutions on Palladium-Covered Platinum Single-Crystal Electrodes, Langmuir. 16 (2000) 4695–4705.

[57] M. Duca, B. van der Klugt, M.T.M. Koper, Electrocatalytic reduction of nitrite on transition and coinage metals, Electrochimica Acta. 68 (2012) 32–43.
[58] R.R. Gadde, S. Bruckenstein, The electroduction of nitrite in 0.1 M $HClO_4$ at platinum, J. Electroanal. Chem. Interfacial Electrochem. 50 (1974) 163–174.